

A modified WKB formulation for linear eigenmodes of a collisionless self-gravitating disc in the epicyclic approximation

Mamta Gulati^{1,2,3,4}, Tarun Deep Saini^{3,5}

¹ *Indian Institute of Science Education and Research Mohali, Chandigarh, 560 012, India*

² *Raman Research Institute, Sadashivanagar, Bangalore 560 080, India*

³ *Indian Institute of Science, Bangalore 560 012, India*

⁴ *mgulati@iisermohali.ac.in*, ⁵ *tarun@physics.iisc.ernet.in*,

21 November 2021

ABSTRACT

The short-wave asymptotics (WKB) of spiral density waves in self-gravitating stellar discs is well suited for the study of the dynamics of tightly-wound wavepackets. But the textbook WKB theory is not well adapted to the study of the linear eigenmodes in a collisionless self-gravitating disc because of the transcendental nature of the dispersion relation. We present a modified WKB of spiral density waves, for collisionless discs in the epicyclic limit, in which the perturbed gravitational potential is related to the perturbed surface density by the Poisson integral in Kalnaj’s logarithmic spiral form. An integral equation is obtained for the surface density perturbation, which is seen to also reduce to the standard WKB dispersion relation. We specialize to a low mass (or Keplerian) self-gravitating disc around a massive black hole, and derive an integral equation governing the eigenspectra and eigenfunctions of slow precessional modes. For a prograde disc, the integral kernel turns out to be real and symmetric, implying that all slow modes are stable. We apply the slow mode integral equation to two unperturbed disc profiles, the Jalali–Tremaine annular discs, and the Kuzmin disc. We determine eigenvalues and eigenfunctions for both $m = 1$ and $m = 2$ slow modes for these profiles and discuss their properties. Our results compare well with those of Jalali–Tremaine.

Key words: methods: analytical — galaxies: kinematics and dynamics — galaxies: nuclei — waves

1 INTRODUCTION

Astrophysical discs display rich structural features such as: double-peak distribution of light in the central regions of galaxies like NGC4486B (elliptical galaxy), and M31 (spiral galaxy) (Lauer et al. 1993, 1996); lopsided brightness distribution of scattered light, warp and clumps in the disc around β Pictoris, which is the second brightest star in the constellation Pictor (Heap et al. 2000; Telesco et al. 2000); spiral structure in HD 141569A (Clampin et al. 2003); clumpy rings in Vega (Marsh et al. 2006), and many more. Structural and kinematic properties of several astrophysical systems have been found to be correlated to the global properties of the system. For example, over a sample of thousands of galaxies, a correlation has been found between the lopsidedness, Black Hole (BH) growth, and the presence of young stellar populations in the center of a galaxy (Reichard et al. 2009). Therefore, the dynamics of these disc-like systems is an important field of investigation.

In this work we will mainly address discs around massive central objects where the self-gravity of the disc is sufficiently weak to make the disc nearly Keplerian. Such discs can support eigenmodes that are slow in comparison to the Keplerian flow. The discs could be gaseous, or particulate and thus collisionless. Sridhar & Saini (2010) & Gulati et al. (2012) studied nearly Keplerian discs by treating the disc as fluid. By assuming that the disc particles interact through softened-gravity, they could mimic the behaviour of collisionless discs. A major limitation of this method is that the fluid discs do not support slow modes for azimuthal wavenumber number $m > 1$. Real collisionless discs, however, can support modes with all values of m (Jalali & Tremaine 2012). Softened gravity discs have also been studied by Tremaine (2001), but with subtle differences in method, as discussed in detail in Gulati et al. (2012).

A general eigenvalue formulation exists for fluid discs, even without assuming the slow mode approximation (Goldreich & Tremaine 1979), although this formulation assumes the tight-winding approximation to make the gravitational potential due to the disc perturbations local. Recently, simulations involving linear perturbations in nearly Keplerian collisionless discs have been performed by Jalali & Tremaine (2012) using the finite element method. However, apart from the disc stability analysis, which gives useful but limited analytical treatment of collisionless discs. In literature there does not exist an eigenvalue formulation for collisionless discs in the WKB approximation (Binney & Tremaine 2008).

In this paper we propose an *eigenvalue formulation of linear perturbations in a collisionless disc* based on the assumptions:

(i) Radial wavenumber k times the radius R is much larger than the azimuthal wavenumber m , i.e. $|kR| \gg m$.

(ii) The epicyclic approximation, in which the velocity dispersion σ_R is much less than the circular speed v_c . We also assume that

$$\frac{\sigma_R}{v_c} \sim \frac{m}{|kR|} \ll 1.$$

The WKB or the tightly-wound spiral approximation requires $|kR| \gg m$, although, in many cases the approximation works fairly well even for $|kR|$ as small as unity (Tremaine 2001; Gulati et al. 2012; Jalali & Tremaine 2012). The gravitational potential for a tightly-wound spiral is local, that is, it can be obtained from the local perturbed density (Binney & Tremaine 2008). However, in our formulation we do not require this assumption, since we use the logarithmic-spiral decomposition of both the perturbed surface density and the gravitational potential (Kalnajs 1971) for solving the Poisson's equation. This allows the potential to take contributions from perturbations across the disc. The integral equation is derived without restricting ourselves to Keplerian discs, and could be used to explore eigenmodes of non-Keplerian discs such as galactic disc. However, to explore the validity of our formulation, for this work we restrict ourselves to nearly Keplerian discs and further approximate the integral equation to the slow mode case to make comparisons with the results of Jalali & Tremaine (2012). As a further test case we also consider perturbations in a Kuzmin disc.

In § 2 we describe the unperturbed disc. The integral equation is derived in § 3. We show in the Appendix A that the integral equation reduces to the standard WKB dispersion relation under the local approximation. We take the *slow mode* limit of the integral equation in § 4 which reduces the equation to a linear eigenvalue problem. In § 5 we describe the numerical method adopted to solve the eigenvalue problem. § 6 gives an account of solutions obtained for two surface density profiles (1) JT annular disc, the disc considered in Jalali & Tremaine (2012) (2) Kuzmin disc. We conclude with general remarks in § 7.

2 UNPERTURBED DISC

Dynamics of disc around a massive compact object, like discs of stars orbiting the supermassive BH found at the center of most galaxies, debris discs etc, are governed by the gravitational potential of the central mass and the self gravity of the disc. In such situations

usually the ratio of disc mass M_d to central mass M (i.e. $\varepsilon \equiv M_d/M$) is much smaller than unity. Orbits of disc particles are nearly Keplerian, and since we neglect relativistic effects the discussion is applicable several Schwarzschild radius away from the central BH. Henceforth we proceed by approximating our disc to be razor-thin, i.e. we restrict ourselves to $z = 0$ plane and work in two spatial dimensions ($\mathbf{r} \equiv (R, \phi)$, cylindrical polar coordinates are used here) .

The potential $\Phi_0(R)$ for the unperturbed disc is given by,

$$\Phi_0(R) = -\frac{GM}{R} + \Phi_d(R), \quad (1)$$

which is a sum of the Keplerian potential due to central mass and gravitational potential due to self gravity of the disc:

$$\Phi_d(\mathbf{r}) = -G \int \frac{\Sigma_d(\mathbf{r}')}{|\mathbf{r} - \mathbf{r}'|} d^2r'. \quad (2)$$

Since disc mass is $O(\varepsilon)$ smaller compared to central mass, so is Φ_d compared to Keplerian potential. Nearly circular orbits have radial frequency κ and azimuthal frequency Ω given by

$$\Omega^2(R) = \frac{GM}{R^3} + \frac{1}{R} \frac{d\Phi_d}{dR}, \quad (3)$$

$$\kappa^2(R) = \frac{GM}{R^3} + \frac{3}{R} \frac{d\Phi_d}{dR} + \frac{d^2\Phi_d}{dR^2}. \quad (4)$$

Such nearly circular orbit precess at a rate given by

$$\begin{aligned} \dot{\omega}(R) &= \Omega(R) - \kappa(R) \\ &= -\frac{1}{2\Omega(R)} \left(\frac{2}{R} \frac{d}{dR} + \frac{d^2}{dR^2} \right) \Phi_d(R) + O(\varepsilon^2). \end{aligned} \quad (5)$$

The unperturbed stellar orbits are considered to be nearly circular. The phase-space coordinates of these epicyclic orbits are given by (Binney & Tremaine 2008);

$$\begin{aligned} R' &= R + \frac{\gamma \tilde{v}_\phi}{\kappa} (1 - \cos(\tau)) + \frac{v_R}{\kappa} \sin(\tau), \\ \phi' &= \phi + \frac{\Omega\tau}{\kappa} + \frac{\gamma\gamma'}{2\kappa} \tilde{v}_\phi \tau + \frac{\gamma}{R\kappa} [\gamma \tilde{v}_\phi \sin(\tau) - v_R (1 - \cos(\tau))], \end{aligned} \quad (6)$$

and

$$\begin{aligned} v'_R &= v_R \cos(\tau) + \gamma \tilde{v}_\phi \sin(\tau), \\ \gamma \tilde{v}'_\phi &= \gamma \tilde{v}_\phi \cos(\tau) - v_R \sin(\tau). \end{aligned} \quad (7)$$

where $\tau = \kappa_g(t' - t)$; $\kappa_g = \kappa(R_g)$; R_g is the mean radius of the orbit for a given angular

momentum; and γ' is the derivative of $\gamma(R) = 2\Omega(R)/\kappa(R)$ w.r.t. R . Also, $\tilde{v}_\phi(R) = v_\phi(R) - v_c(R)$. At $\tau = 0$, the phase-space coordinates $(\mathbf{r}', \mathbf{v}') = (\mathbf{r}, \mathbf{v})$.

The phase space distribution function for the unperturbed collisionless disc in the epicyclic approximation is given by the Schwarzschild distribution function (DF)

$$f_0(R, v_R, \tilde{v}_\phi) = \frac{\gamma \Sigma_d(R)}{2\pi\sigma_R^2} \exp\left(-\frac{v_R^2 + \gamma^2 \tilde{v}_\phi^2}{2\sigma_R^2}\right), \quad (8)$$

where $\Sigma_d(R)$ is the unperturbed surface density profile and σ_R is the radial component of the velocity dispersion.

3 PERTURBED DISC

To study the evolution of small perturbations in this system we begin with perturbing the initial DF such that the distribution function at any time, t is given by,

$$f(R, \phi, v_R, \tilde{v}_\phi, t) = f_0(R, v_R, \tilde{v}_\phi) + f_1(R, \phi, v_R, \tilde{v}_\phi, t). \quad (9)$$

where f_0 is the unperturbed DF, and the perturbation $f_1 \sim \varepsilon f_0$. Hereafter, all perturbed quantities are denoted with a subscript 1 such as X_1 . Perturbations in the surface density are related to the perturbed DF as

$$\Sigma_1(R, \phi, t) = \int f_1(R, \phi, v_R, \tilde{v}_\phi, t) d^2\mathbf{v}, \quad (10)$$

where $d^2\mathbf{v} = dv_R d\tilde{v}_\phi$. The corresponding perturbed potential $\Phi_1(R, \phi, t)$ is

$$\Phi_1(R, \phi, t) = \Phi_1^{\text{dt}}(R, \phi, t) + \Phi_1^{\text{idt}}(R, \phi, t), \quad (11)$$

The term Φ_1^{dt} is the direct term arising due to gravitational interaction between the disc mass particles, and the indirect term Φ_1^{idt} arises since the coordinate system (centered at the massive object) is non-inertial, and is equal to the acceleration of the central mass due to perturbation in the disc. These two terms are given by the Poisson integrals

$$\Phi_1^{\text{dt}}(R, \phi, t) = -G \int_0^\infty \int_0^{2\pi} \frac{\Sigma_1(R', \phi', t) R' dR' d\phi'}{\sqrt{R^2 + R'^2 - 2RR' \cos(\phi - \phi')}}}, \quad (12)$$

and

$$\begin{aligned} \Phi_1^{\text{idt}}(R, \phi, t) &= GR \int_0^\infty \int_0^{2\pi} \frac{\Sigma_1(R', \phi', t) \cos(\phi - \phi') dR' d\phi'}{R'}, \\ &= \pi GR (\delta_{m,1} + \delta_{m,-1}) \exp[i(m\phi - \omega t)] \int_0^\infty \frac{\Sigma_a(R')}{R'} dR'. \end{aligned} \quad (13)$$

The second form of the indirect term in the above equation is applicable if the perturbations are of the form $\Sigma_1(R', \phi', t) = \Sigma_a(R') \exp[i(m\phi' - \omega t)]$, and is given here for later use.

The linearised collisionless Boltzman equation (CBE) is given by

$$\frac{df_1}{dt} = - [f_0, \Phi_1] , \quad (14)$$

where the time derivative on the left hand side is computed along the unperturbed orbit, and the bracket $[*, *]$ on the right hand side is the Poisson bracket. The solution of linearised CBE is given by

$$f_1(R, \phi, v_R, \tilde{v}_\phi, t) = - \int_{-\infty}^t dt' [f_0, \Phi_1]_{\mathbf{x}', \mathbf{v}', t'} , \quad (15)$$

where $(\mathbf{x}', \mathbf{v}') = (R', \phi', v'_R, \tilde{v}'_\phi)$ are given by Eqs. (6) and (7).

We seek solutions of the perturbed quantities for which ϕ and t dependence of the perturbed quantities goes as $\exp[i(m\phi - \omega t)]$. The perturbation is assumed to vanish at $t \rightarrow -\infty$, which formally requires ω to have a non-zero positive imaginary part however small it may be. Expanding the Poisson bracket gives

$$[f_0, \Phi_1] = - \frac{\partial f_0}{\partial \mathbf{v}} \cdot \nabla \Phi_1 . \quad (16)$$

Combining this with Eqn. (10), (11), and (15) we can obtain the perturbed density due to the direct and indirect terms in the potential as

$$\Sigma_a(R) = \Sigma_a^{\text{dt}}(R) + \Sigma_a^{\text{idt}}(R) , \quad (17)$$

where

$$\Sigma_a^* = \exp[-i(m\phi - \omega t)] \int_{-\infty}^{\infty} \int_{-\infty}^{\infty} dv_R d\tilde{v}_\phi \int_{-\infty}^t dt' \left[\frac{\partial f_0}{\partial \mathbf{v}} \cdot \nabla \Phi_1^* \right]_{\mathbf{x}', \mathbf{v}', t'} , \quad (18)$$

where $*$ stands for ‘dt’ or ‘idt’. The next section is dedicated to solving the above set of equations, by substituting for Φ_1^{dt} and Φ_1^{idt} to derive the integral-equation for Σ_a .

3.1 The Integral Equation

We use the log-spiral expansion of surface density and potential (Kalnajs 1971; Binney & Tremaine 2008) to write Φ_1^{dt} in Eqn. (18) in terms of Σ_a :

$$\Phi_1^{\text{dt}}(R, \phi, t) = - \frac{G}{R^{1/2}} \int_{-\infty}^{\infty} \frac{d\alpha}{2\pi} N(\alpha, m) A_m(\alpha) e^{i(\alpha q + m\phi - \omega t)} , \quad (19)$$

where $q = \ln R$, and

$$A_m(\alpha) = \int_{-\infty}^{\infty} dq' R'^{3/2} \Sigma_a(R') e^{-i\alpha q'} , \quad (20)$$

$$N(\alpha, m) = \pi \frac{\Gamma(z) \Gamma(z^*)}{\Gamma(z + \frac{1}{2}) \Gamma(z^* + \frac{1}{2})} , \quad (21)$$

where $z = m/2 + 1/4 + i\alpha/2$. Using this solution for $\Phi_1^{\text{dt}}(R, \phi, t)$ and the expression for $f_0(R, v_R, \tilde{v}_\phi)$ given in Eq. (8) we get

$$\begin{aligned} \frac{\partial f_0}{\partial \mathbf{v}} \cdot \nabla \Phi_1^{\text{dt}} \Big|_{\mathbf{x}', \mathbf{v}', t'} &= \frac{G f_0(R, v_R, \tilde{v}_\phi)}{R^{3/2} \sigma_R^2} \exp[i(m\phi - \omega t)] \int_{-\infty}^{\infty} \frac{d\alpha}{2\pi} \times \\ &\times \left[\left(i\alpha - \frac{1}{2} \right) v_R + im\gamma^2 \tilde{v}_\phi \right] N(\alpha, m) A_m(\alpha) e^{i\alpha q} \Big|_{\mathbf{x}', \mathbf{v}', t'}. \end{aligned} \quad (22)$$

Substituting the above in the expression for Σ_a^{dt} given by Eq. (18) we get

$$\begin{aligned} \Sigma_a^{\text{dt}}(R) &= \frac{G}{R^{3/2} \sigma_R^2} \exp[-i(m\phi - \omega t)] \int_{-\infty}^{\infty} \frac{d\alpha}{2\pi} N(\alpha, m) A_m(\alpha) \times \\ &\times \int_{-\infty}^{\infty} \int_{-\infty}^{\infty} dv_R d\tilde{v}_\phi f_0 \int_{-\infty}^t dt' \exp[i(\alpha q' + m\phi' - \omega t')] \times \\ &\times \left[v'_R \left(i\alpha - \frac{1}{2} \right) + im\gamma^2 \tilde{v}'_\phi \right]. \end{aligned} \quad (23)$$

The above equation has been derived under the standard WKB approximations. For details refer to the Appendix K of Binney & Tremaine (2008). The main approximations made are:

(i) We retain terms up to first order in small parameter $|R' - R|$, which is on the order of the epicyclic amplitude.

(ii) Also, to a good approximation we can write $|R' - R| \ll R$, and hence any slowly varying function of R' such as $\sigma_R(R')$, $\gamma(R')$, $\Sigma_d(R')$, can be replaced by their values at R and taken out of the integral.

(iii) Since $q' = \ln(R') = \ln(R + \delta R)$, up to first order $q' = q + (\delta R/R)$.

(iv) We assume that $|\alpha| \gg m$, and we keep only leading order terms in α at each step. This is the equivalent condition to the standard WKB approximation as will be proved in the Appendix A. For large α , the leading order radial oscillations of phase are balanced by the (unperturbed) drift of ϕ at the rate Ω , while the epicyclic drift and oscillations of ϕ may be neglected. Also in the linear term, i.e. the term outside the exponent, only $i\alpha v'_R$ term contributes.

Defining $s = (\omega - m\Omega)/\kappa$, $u = v_R/\sigma_R$ and $v = \gamma \tilde{v}_\phi/\sigma_R$, and substituting the expressions for v'_R , \tilde{v}'_ϕ and ϕ' from equations (6)–(7) in the above integral, we get

$$\Sigma_a^{\text{dt}}(R) = \frac{G \Sigma_d}{2\pi R^{3/2} \kappa \sigma_R} \int_{-\infty}^{\infty} \frac{d\alpha}{2\pi} N(\alpha, m) A_m(\alpha) e^{i\alpha q} \int_{-\infty}^0 d\tau \exp[-is\tau] \mathcal{A}, \quad (24)$$

We have defined $\tau = \kappa_g(t' - t)$, and

$$\mathcal{A} = \int_{-\infty}^{\infty} \int_{-\infty}^{\infty} du dv (au + bv) \exp \left[-\frac{u^2 + v^2}{2} + i(cu + dv) \right]; \quad (25)$$

$$a = i\alpha \cos \tau, \quad b = i\alpha \sin \tau, \quad c = \frac{\sigma_R}{R\kappa} \alpha \sin \tau, \quad \text{and} \quad d = \frac{\sigma_R}{R\kappa} \alpha (1 - \cos \tau). \quad (26)$$

Since v_R and \tilde{v}_ϕ are small on the order of the epicyclic amplitude, we replace κ_g with $\kappa(R)$ in Eq. (24). Solving the integrals in \mathcal{A} , it can be brought to the form

$$\mathcal{A} = -\frac{2\pi\sigma_R}{R\kappa} \alpha^2 \sin \tau \exp[-\chi(1 - \cos(\tau))] , \quad (27)$$

where $\chi = \sigma_R^2 \alpha^2 / R^2 \kappa^2$. Combining Eqs. (24) and (27), expression for $\Sigma_a^{\text{dt}}(R)$ reduces to

$$\Sigma_a^{\text{dt}}(R) = -\frac{G\Sigma_d}{R^{5/2}\kappa^2} \int_{-\infty}^{\infty} \frac{d\alpha}{2\pi} N(\alpha, m) A_m(\alpha) \alpha^2 e^{i\alpha q} \mathcal{I}_1(s, \chi) , \quad (28)$$

where

$$\mathcal{I}_1(s, \chi) = \int_{-\infty}^0 d\tau \sin \tau \exp[-is\tau - \chi(1 - \cos \tau)] , \quad (29)$$

The algebra required to obtain \mathcal{I}_1 closely follows the Appendix-K of Binney & Tremaine (2008). The final result is

$$\mathcal{I}_1(s, \chi) = -\frac{2e^{-\chi}}{\chi} \sum_{n=1}^{\infty} \left(\frac{n^2}{n^2 - s^2} \right) I_n(\chi) . \quad (30)$$

Substituting for \mathcal{I}_1 in Eq. (28) and simplifying gives

$$\Sigma_a^{\text{dt}}(R) = \frac{2G\Sigma_d}{R^{5/2}\kappa^2} \sum_{n=1}^{\infty} \left(\frac{n^2}{n^2 - s^2} \right) \int_{-\infty}^{\infty} \frac{d\alpha}{2\pi} N(\alpha, m) A_m(\alpha) e^{i\alpha q} B_n(\alpha, \chi) . \quad (31)$$

Here $B_n(\alpha, \chi)$ is defined as

$$B_n(\alpha, \chi) = \frac{\alpha^2}{\chi} e^{-\chi} I_n(\chi) . \quad (32)$$

Note that

(i) $B_n(\alpha, \chi)$ is an even function of α . This property will be useful while calculating the integral over α , as we shall see later.

(ii) To leading order in α , B_n is proportional to α^2 .

Having expressed Σ_a^{dt} in the desired form given by Eqn. (31), we now turn to the calculation of Σ_a^{idt} . Below we prove that to leading order $\Sigma_a^{\text{idt}} = 0$. $\Phi_1^{\text{idt}}(R, \phi, t)$, as given in Eq. (13), can be rewritten as

$$\Phi_1^{\text{idt}}(R, \phi, t) = R \exp[i(m\phi - \omega t)] \mathcal{I}_m ,$$

where, $\mathcal{I}_m = \pi G(\delta_{m,1} + \delta_{m,-1}) \int_0^{\infty} \frac{dR'}{R'} \Sigma_a(R') ,$ (33)

is a constant. Using this we can write

$$\frac{\partial f_0}{\partial \mathbf{v}} \cdot \nabla \Phi_1^{\text{idt}} \Big|_{\mathbf{x}', \mathbf{v}', t'} = -\frac{f_0}{\sigma_R^2} \exp[i(m\phi' - \omega t')] (v'_R + im\gamma^2 \tilde{v}'_\phi) \mathcal{I}_m . \quad (34)$$

Combining Eqs. (18) and (34) and defining s, τ, u and v as done before Σ_a^{idt} becomes

$$\Sigma_a^{\text{idt}} = -\frac{\mathcal{I}_m \Sigma_d}{2\pi\kappa\sigma_R} \int_{-\infty}^0 d\tau e^{-is\tau} \mathcal{A}' , \quad (35)$$

where

$$\mathcal{A}' = \int_{-\infty}^{\infty} \int_{-\infty}^{\infty} du dv (a'u + b'v) \exp \left[-\frac{u^2 + v^2}{2} \right], \quad (36)$$

$$a' = \cos \tau - im\gamma \sin \tau,$$

$$b' = \sin \tau + im\gamma \cos \tau. \quad (37)$$

In writing the above integral we have neglected the oscillations in ϕ and the epicyclic drift term. Neglecting these terms involves the same level of approximation as in calculating Σ_a^{dt} . The integral in \mathcal{A}' is exactly equal to zero since the integrand is an odd functions of u and v , therefore

$$\Sigma_a^{\text{idt}} = 0. \quad (38)$$

As given in Eq. (17), Σ_a is the sum of both Σ_a^{dt} and Σ_a^{idt} . Combining Eqs. (17), (20), (31), and (38) we get

$$\Sigma_a(R) = \frac{G\Sigma_d}{R^{5/2}\kappa^2} \int_{-\infty}^{\infty} dq' \mathcal{G}_m(s, \chi, q - q') R'^{3/2} \Sigma_a(R'), \quad (39)$$

where

$$\mathcal{G}_m(s, \chi, q) = 2 \sum_{n=1}^{\infty} \left(\frac{n^2}{n^2 - s^2} \right) \int_{-\infty}^{\infty} \frac{d\alpha}{2\pi} N(\alpha, m) B_n(\alpha, \chi) e^{i\alpha q}. \quad (40)$$

We have already discussed that both the functions $N(\alpha, m)$ and $B_n(\alpha, \chi)$ are even functions of α . Since ‘ $\sin(\alpha q)$ ’ and ‘ $\cos(\alpha q)$ ’ are odd and even functions of ‘ α ’ respectively, only ‘ \cos ’ term in the integral over α survives. Combining these, the integral equation reduces to,

$$\mathcal{S}(R) = \int_{-\infty}^{\infty} dq' \left[\frac{\mathcal{C}(R)\mathcal{C}(R')}{\kappa(R)} \mathcal{G}_m(s, \chi, q - q') \right] \mathcal{S}(R'), \quad (41)$$

where

$$\mathcal{G}_m(s, \chi, q) = 4 \sum_{n=1}^{\infty} \left(\frac{n^2}{n^2 - s^2} \right) \int_0^{\infty} \frac{d\alpha}{2\pi} N(\alpha, m) B_n(\alpha, \chi) \cos(\alpha q). \quad (42)$$

and we have defined

$$\mathcal{S}(R) = \frac{R^{3/2}\Sigma_a(R)}{\mathcal{C}(R)} \quad \text{and} \quad \mathcal{C}(R) = \sqrt{\frac{G\Sigma_d(R)}{R\kappa(R)}}. \quad (43)$$

Equation (41), together with the functions defined in Eq. (42) & (43) is the integral eigenvalue problem for tightly-wound linear modes of an axisymmetric disc in the epicyclic approximation. The application of this equation is not restricted to Keplerian discs, it could also be used to explore modes of non-Keplerian discs such as galactic disc. We show in Appendix A that the local limit of this equation gives the same dispersion relation as is used for stellar discs (Binney & Tremaine 2008).

4 THE SLOW MODE LIMIT

The general integral equation, Eqn. 41, derived in the previous section is difficult to solve in its standard form due to the presence of an infinite series. The near equality of Ω and κ for nearly Keplerian discs has a simplifying effect on this equation. For such discs, $\Omega(R) = \kappa(R) + \dot{\varpi}$, and $\dot{\varpi} \sim O(\varepsilon)$. If we make an ansatz that the eigenfrequency $\omega \sim O(\varepsilon) \ll 1$, then we find that $s \simeq -m$, $\gamma \simeq 2$ to leading order and

$$m^2 - s^2 = \frac{2m(\omega - m\dot{\varpi})}{\kappa}. \quad (44)$$

Therefore, in the summation over n from 1 to ∞ in Eq. (42), $n = m$ term dominates due to the presence of the factor $1/(n^2 - s^2)$. Note that there is no restriction on m , and slow modes exist for all m . The magnitude of the frequencies obtained later in the paper indeed satisfies this ansatz, thereby validating the slow mode approximation.

Further simplification is possible if we take $\sigma_R(R) = \sigma R\kappa(R)$, where σ is a dimensionless constant less than unity. Using such a profile means that the radial profile of σ_R is same as $R\kappa(R) \simeq R\Omega(R) = v_c(R)$. The epicyclic condition is satisfied for $\sigma < 1$, which is one of the fundamental assumption that has gone into deriving the integral equation. Moreover, Jalali & Tremaine (2012) have studied a specific problem with this simplifying assumption for σ_R . Therefore, it is convenient to use this in our formulation to compare results obtained by them using our integral equation for validation of our equation.

Since we have assumed σ to be constant, χ is also a constant, leading to considerable simplification. Using these simplifying assumptions in Eqs. (41)–(43) we obtain

$$\omega \mathcal{S}(R) = m\dot{\varpi}(R)\mathcal{S}(R) + \int_{-\infty}^{\infty} dq' \mathcal{H}_m(\sigma, q, q') \mathcal{S}(R'), \quad (45)$$

where the kernel

$$\mathcal{H}_m(\sigma, q, q') = 2m \mathcal{C}(R)\mathcal{C}(R') \int_0^{\infty} \frac{d\alpha}{2\pi} N(\alpha, m) B_m(\alpha, \chi) \cos(\alpha(q - q')). \quad (46)$$

This is the integral eigenvalue problem for slow modes in a nearly Keplerian collisionless disc. Note that the kernel of the integral equation is symmetric in R and R' (or q and q'). Hence the integral operator on the RHS can be regarded as a linear Hermitian operator. Properties of Hermitian operators imply that the eigenvalues ω are all real, *thus all slow modes are stable*. Also, the eigenfunctions $\mathcal{S}(R)$ can be assumed to be real.

5 NUMERICAL METHOD

In this section we discuss the numerical methods used to solve the above derived integral equation. First step is to solve for $\mathcal{H}_m(\sigma, q, q')$. We define the function K_m

$$K_m(\sigma, q) = \int_0^\infty \frac{d\alpha}{2\pi} N(\alpha, m) B_m(\alpha, \chi) \cos(\alpha q), \quad (47)$$

in terms of which the kernel $\mathcal{H}_m(\sigma, q, q')$ takes the form

$$\mathcal{H}_m(\sigma, q, q') = 2m \mathcal{C}(R) \mathcal{C}(R') K_m(\sigma, q - q'). \quad (48)$$

Calculation of K_m involves integral over α , the function $N(\alpha, m)$, and $B_m(\alpha, \chi)$.

The functional form of $B_m(\alpha, \chi)$ contains the combination $e^{-\chi} I_m(\chi)$ and we calculate this instead of I_m because I_m increases exponentially for large value of its argument. Next we tabulate $N(\alpha, m)$ as a function of α for a given value of m . Using the identities $\Gamma(z^*) = \Gamma(z)^*$ and $zz^* = |z|^2$, the expression for $N(\alpha, m)$ in Eq. (21) becomes

$$N(\alpha, m) = \pi \left| \frac{\Gamma(z)}{\Gamma(z + \frac{1}{2})} \right|^2. \quad (49)$$

We then use the following identity to calculate $|\Gamma(x + iy)|$:

$$|\Gamma(x + iy)| = |\Gamma(x)| \prod_{n=0}^{\infty} \left[\frac{(x+n)^2 + y^2}{(x+n)^2} \right]^{-1/2}. \quad (50)$$

Taking log on both sides converts the product into summation. Convergence of series over n is achieved iteratively till the accuracy of 10^{-8} is attained, and then we exponentiate to obtain $\Gamma(x + iy)$. Also $|\Gamma(x + iy)|$ is a decreasing function of y , and since we need to evaluate $|\Gamma(x + iy)/\Gamma(x + iy + 1/2)|$ as a function of y , when the minimum of machine precision is reached, $N(\alpha, m)$ becomes indeterminate. We avoid this by using the asymptotic form of this function given in Eq. (A7).

The function K_m is next calculated by evaluating the integral over α by using the Gaussian quadrature. Although the integrand becomes small for large values of α , but due to the presence of oscillatory cosine function the tail of the integrand has to be handled carefully. The integral evaluated up to infinity ensures complete cancellation due to oscillatory functions, however since we evaluate the integral numerically up to a finite range in α , we have to deal with small spurious contributions from the tail. To avoid this we take α range to be quite high. For typical maximum value of $\alpha_{\max} = e^{25-27}$, and number of grid points, in $\log(\alpha)$ scale, $N_\alpha = 10^7$, the function K_m converges to sixth or seventh decimal place.

In our calculation the variables q and q' are assigned the range $[-6, 6]$, which is divided into 4000 points each. The lower range of q is chosen to avoid numerical singularities for $q \rightarrow -\infty$. Also, the upper limit is chosen since the surface density decreases substantially

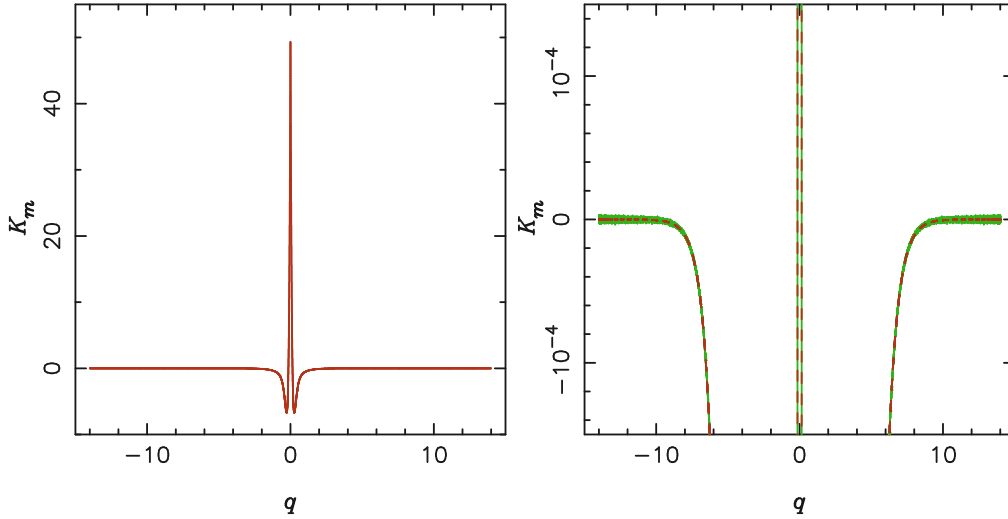


Figure 1. Plot of K_m vs q for $m = 1$, $\sigma = \sigma_R/R\kappa(R) = 0.1$. Left panel is the plot of smoothed K_m and the right panel displays the zoom of y -axis for a window of -1.5×10^{-4} to 1.5×10^{-4} . Green one is the original curve whereas red one is after doing a box-smoothing.

beyond $q = 6$. These enter K_m in the combination $q - q'$ which then ranges from -12 to 12 . We first tabulate K_m as a function of ‘ q ’ ranging from -14 to 14 with a grid size of 10^5 for a given value of ‘ m & σ ’ as defined in Eqn. (47). The range is extended from $[-12, 12]$ to $[-14, 14]$ just to make sure that tail effects are minimized. As we have discussed earlier there is numerical noise in the tail of the integral over α due to the presence of oscillatory functions. To reduce the noise we do a box smoothing for K_m , which works quite well. In Fig. 1 we display a plot of K_m as a function of q . The left panel is the plot of box smoothed K_m and the right panel is zoom of y -axis from -1.5×10^{-4} to 1.5×10^{-4} . The green curve is the unsmoothed curve and the red curve is the smoothed curve. The reduction in numerical noise can be easily seen in this figure.

Having once tabulated K_m as a function of q for a given m and σ , we divide $-6 \leq q$ (and $q') \leq 6$ into a grid of n_q points and interpolate the tabulated function to calculate actual matrix entries. Further, the calculation of \mathcal{H}_m , once we have K_m , involves calculation of simple algebraic functions only. The discretization of the integral over q' in Eqn. (45) follows the scheme

$$\int_{-\infty}^{\infty} dq' \mathcal{H}_m(\sigma, q_i, q') \mathcal{S}(q') \quad \longrightarrow \quad \sum_{j=1}^{n_q} w_{q_j} \mathcal{H}_m(\sigma, q_i, q_j) \mathcal{S}(q_j), \quad (51)$$

where we have divided q (and q') on a grid of n_q points using the Gaussian quadrature rule, and w_{q_j} are the appropriate weights. Using this, the discretized integral-equation can be

written as

$$\mathbf{A}\mathcal{S} = \omega\mathcal{S}, \quad (52)$$

where \mathbf{A} is a $n_q \times n_q$ matrix defined as

$$\mathbf{A} = \left[w_{q_j} \mathcal{H}_m(\sigma, q_i, q_j) + m\dot{\omega}_i \delta_{ij} \right]. \quad (53)$$

Row and column indices are i and j , respectively. Note that no summation is implied over repeated indices. The presence of unequal weights makes the matrix non-symmetric. Since the weights are all positive, the symmetry is easily restored by the transformation given in § 18.1 of Press et al. (1992). We write $\tilde{\mathcal{H}}_m = \mathcal{H}_m \mathbf{D}$, where $\mathbf{D} = \text{diag}(w_{q_j})$. Now

$$\begin{aligned} \mathbf{D}^{1/2} \tilde{\mathcal{H}}_m \mathcal{S} &= (\mathbf{D}^{1/2} \mathcal{H}_m \mathbf{D}^{1/2}) \mathbf{D}^{1/2} \mathcal{S}, \\ &= (\mathbf{D}^{1/2} \mathcal{H}_m \mathbf{D}^{1/2}) \mathbf{h}, \end{aligned} \quad (54)$$

where $\mathbf{h} = \mathbf{D}^{1/2} \mathcal{S}$ and $\mathbf{D}^{1/2} = \text{diag}(\sqrt{w_{q_j}})$. We use this as our input to calculate the eigenvalues and eigenfunctions (which now is \mathbf{h}) numerically rather than $\tilde{\mathcal{H}}_m$, which is originally there in matrix \mathbf{A} . And then restore \mathcal{S} by using the transformation $\mathcal{S} = \mathbf{D}^{-1/2} \mathbf{h}$, where $\mathbf{D}^{-1/2} = \text{diag}(1/\sqrt{w_j})$. We have used the linear algebra package LAPACK (Anderson et al. 1999) to calculate eigenvalues and eigenvectors.

6 NUMERICAL RESULTS

We consider two contrasting models of the disc density to explore the possible eigenvalues and eigenfunctions of the slow modes. Both the models contain a characteristic disc scale-length ‘ a ’, which we use to cast the equations in a dimensionless form. R/a is the dimensionless radius; and to convert other physical quantities to dimensionless form we use M_d/a^2 as the characteristic surface density and $\Omega^* = \sqrt{GM/a^3}$ as the characteristic orbital frequency. The net effect is that the dimensionful eigenfrequencies ω are obtained from the dimensionless frequencies by multiplying with $(\Omega^* a^3 / GM_d)^{-1}$. In the rest of the paper the notation (R , Σ_d , ω , Ω and $\mathcal{C}(R)$, etc), used earlier for dimensionful quantities, will stand for dimensionless quantities. The two discs models considered for our numerical exploration are:

(i) **JT annular disc**: This is an annular disc model around the central massive object obtained by subtracting two Toomre discs (Toomre 1963). This profile was analyzed for slow modes by Jalali & Tremaine (2012) by solving the collisionless Boltzmann equation in the ring-ring interaction approximation. Since the eigenvalues for this problem are known, this model also serves to validate our eigenequation. Following them we call the disc JT annular

disc. The radial profile (dimensionless form) is given by

$$\Sigma_d^{\text{JT}}(R) = \frac{3}{4\pi} \left[\frac{1}{(1+R^2)^{3/2}} - \frac{1}{(1+R^2)^{5/2}} \right] = \frac{3R^2}{4\pi(1+R^2)^{5/2}}, \quad (55)$$

And the corresponding precession rate for nearly circular orbits is

$$\dot{\omega}^{\text{JT}}(R) = \frac{3(1-4R^2)}{4\Omega(R)(1+R^2)^{7/2}}. \quad (56)$$

Note that $\Omega(R)$ used here is the dimensionless azimuthal frequency. $\dot{\omega}^{\text{JT}}(R) > 0$ for $0 < R < 1/2$, zero at $R = 1/2$ and negative thereafter. Positive and negative maxima are 0.05861 and -0.2078 , respectively. Both $\Sigma_d^{\text{JT}}(R)$ and $\dot{\omega}^{\text{JT}}(R)$ are plotted in the left panel of Fig. 2.

(ii) **Kuzmin disc:** Several earlier investigations of slow modes (Tremaine 2001; Sridhar & Saini 2010; Gulati et al. 2012) have considered the Kuzmin disc model. We consider this model to make comparison with the earlier works. The surface density and the precession frequency for a Kuzmin disc are

$$\Sigma_d^{\text{Kz}}(R) = \frac{1}{2\pi(1+R^2)^{3/2}}, \quad (57)$$

$$\dot{\omega}^{\text{Kz}}(R) = \frac{-3}{2\Omega(R)(1+R^2)^{5/2}}. \quad (58)$$

Both the quantities are in dimensionless units. Note that $\dot{\omega}^{\text{Kz}} \leq 0$ for all values of R . We plot both $\Sigma_d^{\text{Kz}}(R)$ and $\dot{\omega}^{\text{Kz}}(R)$ in the right panel of Fig. 2.

These profiles differ from each other: (1) Surface density for Kuzmin disc is centrally concentrated whereas for JT annular disc is concentrated about $R = 1$. (2) Precession frequency is negative throughout for Kuzmin disc, whereas for JT annular disc it starts from zero, attains a positive maxima, becomes negative, reaches a minimum, and then goes to zero. We give and compare the results from both these profiles next.

6.1 JT annular Disc

We present results for $m = 1$ and 2 , with $\sigma = 0.1, 0.2, 0.3$ & 0.4 . Both continuous as well as discrete eigenfrequencies are supported by the eigenequation. The continuous spectrum, however, has singular eigenfunctions where the eigenfrequencies are $\omega = m\dot{\omega}$. The plot of the more interesting discrete eigenvalues for JT annular disc is given in Fig. 3. The X-axis is the dimensionless pattern speed, $\Omega_p = \omega/m\omega_0$, where $\omega_0 = 0.05861$ is positive maxima of precession frequency. Note that all frequencies are measured in the units of ' $\varepsilon\sqrt{GM/a^3}$ ', the natural slow mode frequency. The Y-axis is σ , which is a dimensionless measure of the heat in the disc. We note the following trends from Fig. 3 for $m = 1$ and $m = 2$ modes:

- (i) The modes are all stable with prograde pattern speeds $\Omega_p > 1$.

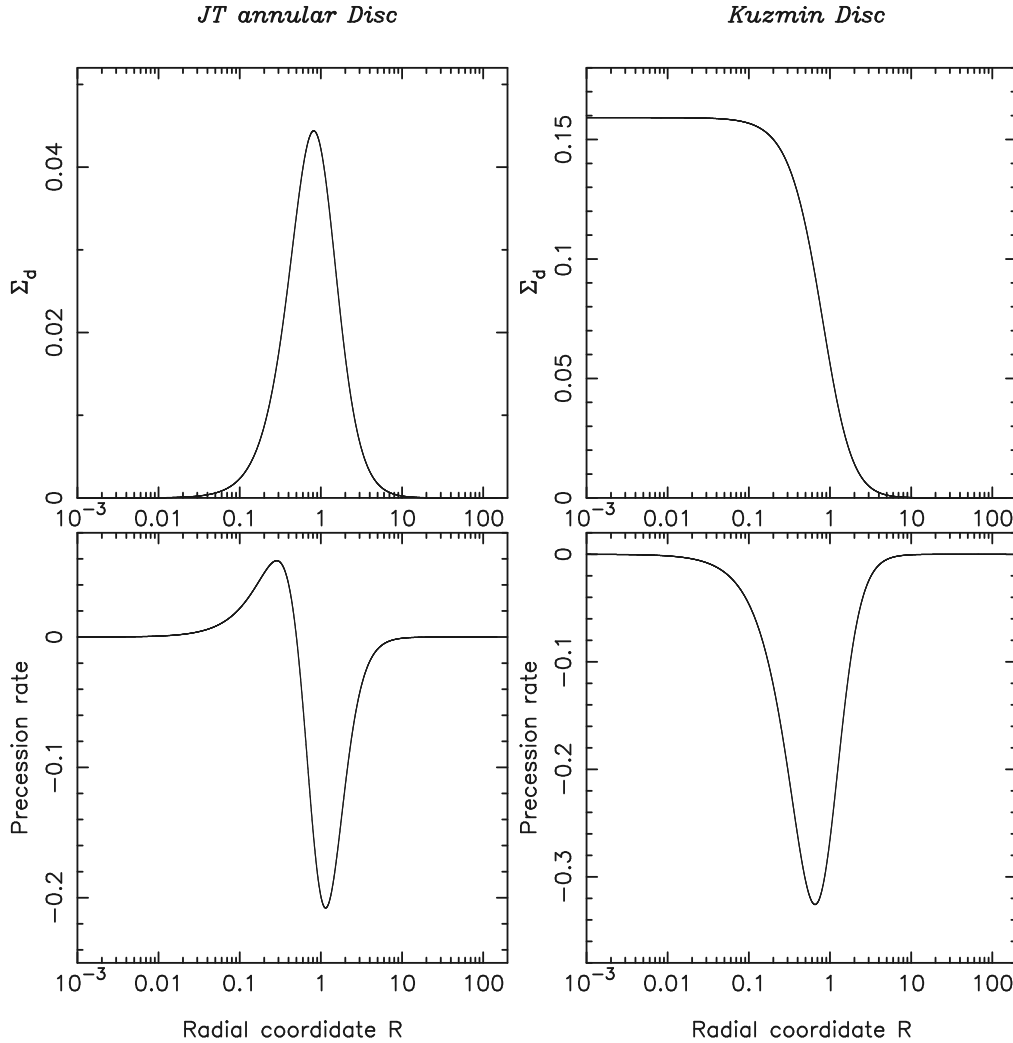


Figure 2. Surface density and precession frequency profiles for JT annular disc and Kuzmin disc are displayed. Panels on the left correspond to JT annular disc and those on the right are the profiles for Kuzmin disc. Top row displays the surface density, Σ_d , and the bottom one are the plots for the precession rate $\dot{\varphi}$.

(ii) For given (σ, m) , the pattern speed belongs to a discrete spectrum. Let $\Omega_{\max}(\sigma, m)$ be the largest eigenvalue of this spectrum. Then

- (a) At fixed m , Ω_{\max} is a decreasing function of σ .
- (b) At fixed σ , $\Omega_{\max}(\sigma, 1) > \Omega_{\max}(\sigma, 2)$.

Plot for $m = 1$ is to be compared with Fig. 4 of Jalali & Tremaine (2012). Mean eccentricity used by the authors is linearly proportional to σ used in the present work. Apart from the last property of the eigenspectra mentioned above (about which nothing has been said by the authors), our conclusions are consistent with their results. Eigenvalues match within a few percent which Jalali & Tremaine get by solving collisionless Boltzmann equation, and even better with the eigenvalues obtained after solving the local WKB dispersion relation. All the eigenvalues with $\Omega_p \leq 1$ that we get are singular for all the values of σ .

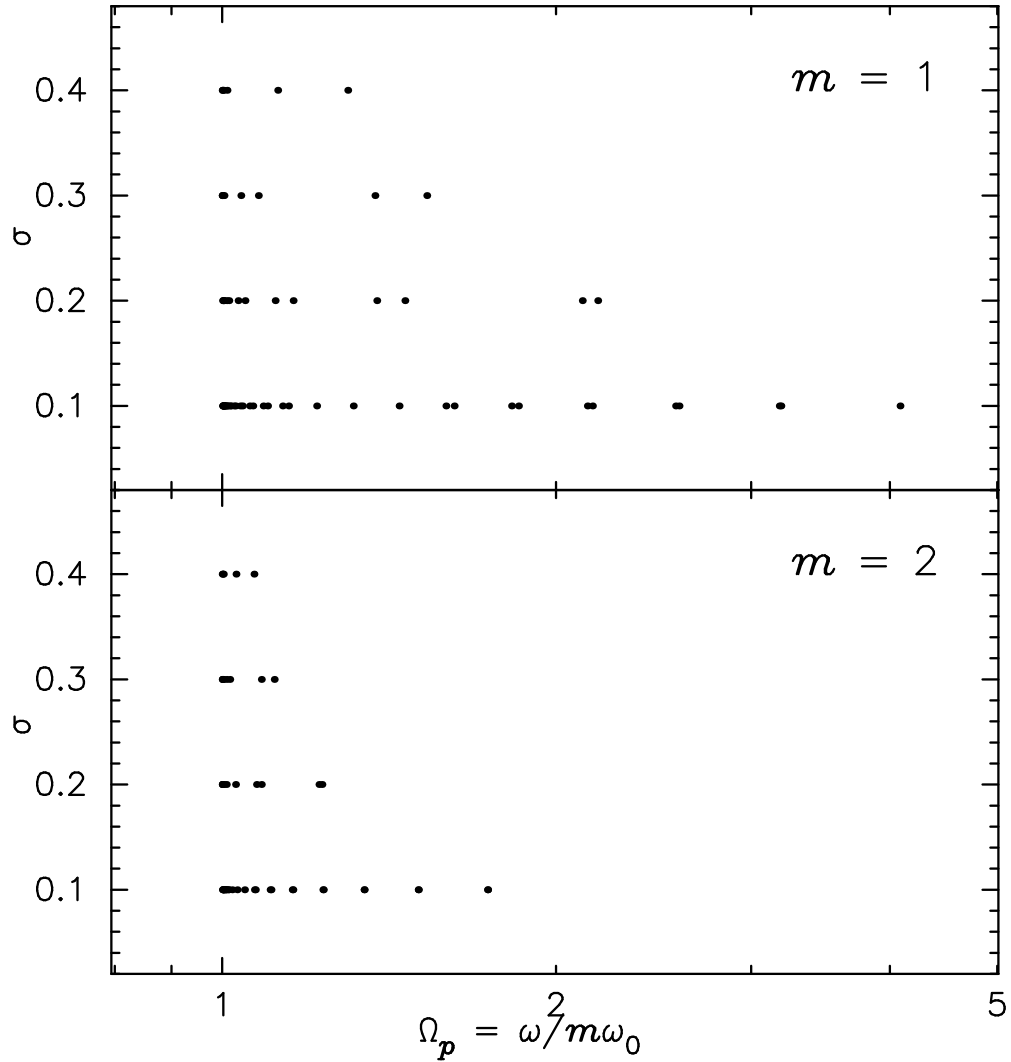


Figure 3. Non-singular eigenfrequencies for JT annular disc profile for $m = 1$ & 2 and $\sigma = 0.1, 0.2, 0.3$ and 0.4 . Eigenvalues are all real and prograde. X-axis is $\Omega_p = \omega/m\omega_0$, where ω_0 is the positive maxima of precession rate and Y-axis is the σ value. Plots are labelled for their respective m values.

Figure 4 and 6 show the radial profile of $\Sigma_a(R)$ for $m = 1$ and 2 , respectively. Functions are normalized such that $\int dq \Sigma_a^2(R) = 1$. We plot the eigenfunctions for the first two eigenvalues for all the values of σ . Panels are labelled for the values σ and Ω_p . Number of nodes increase as the Ω_p value decreases. In Fig. 5 and 7 we plot the image of oscillatory patterns of the positive part of $\Sigma_a(R) \cos(m\phi)$ for $m = 1$ and 2 , respectively, which is essentially the positive component of the real part of $\Sigma_1(R, \phi, t)$ at $t = 0$. Plots for the highest values of Ω_p are displayed and their respective σ values are given in the panels. Surface density is normalized to unity in all the panels. Contours range from 0 to 1, and the corresponding colors are shown in a wedge on the right side. Wavepackets are more radially compact for lower values of σ .

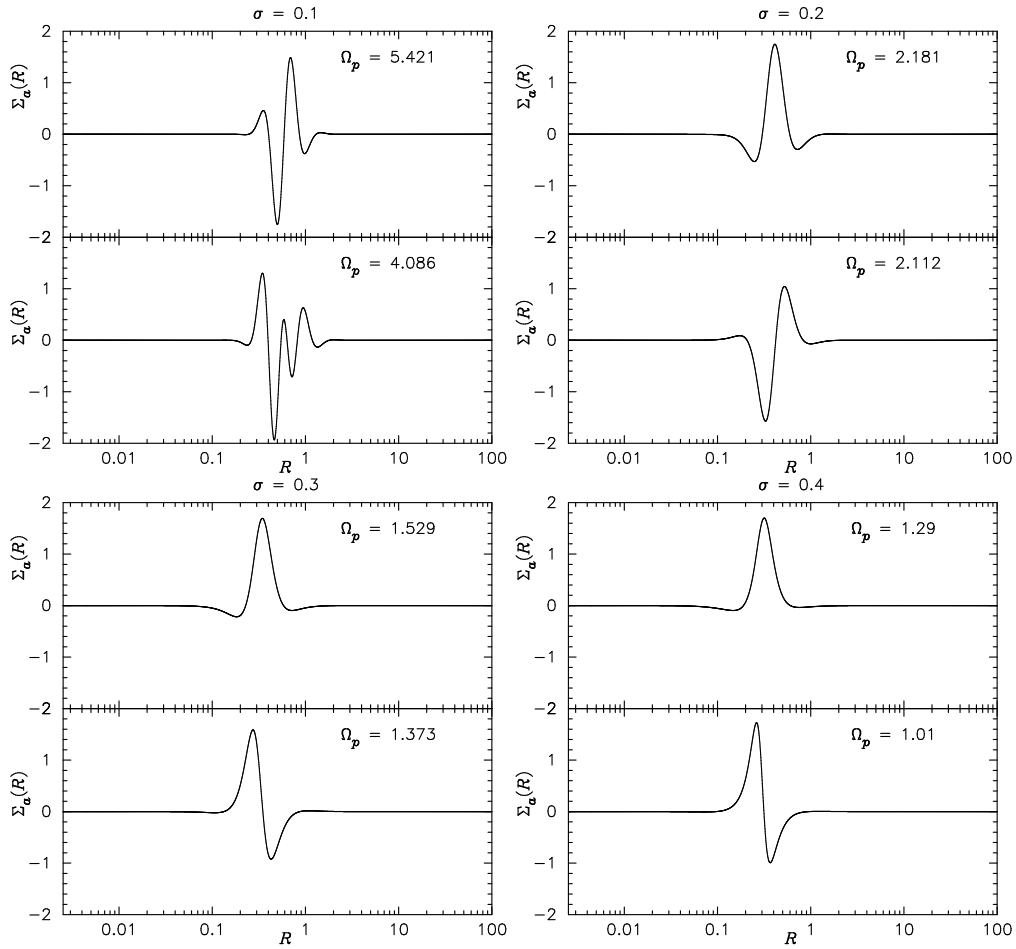


Figure 4. Plot of perturbed surface density, $\Sigma_a(R)$ as a function of R for $m = 1$ and JT annular disc profile. Eigenfunctions for first two eigenvalues for each value of σ are displayed. Panels are labelled for the values of σ and Ω_p . Functions are square normalized to unity such that $\int dq \Sigma_a^2(R) = 1$.

6.2 Kuzmin disc

In this subsection we present the results for Kuzmin disc profile. Eigenspectrum we get in this case also is composed of singular modes given by $\omega = m\dot{\omega}$ and the non-singular eigenvalues. Figure 8 gives the plot of non-singular eigenvalues for the Kuzmin disc. We have plotted for $m = 1$ & 2 and $\sigma = 0.1, 0.2, 0.3$ and 0.4. Horizontal axis is $\Omega_p = \omega/m\omega_0$, where ω_0 is the maxima of $|\dot{\omega}|$ rather than positive maxima (as used for the JT disc) because for Kuzmin disc $\dot{\omega}(R) \leq 0$. We note the following trends in the eigenspectrum for $m = 1$ and $m = 2$:

(i) Eigenmodes are stable with prograde pattern speeds $\Omega_p > 0$, in contrast to JT disc where $\Omega_p > 1$.

(ii) For a given value of m , Ω_{\max} is a decreasing function of σ and $\Omega_{\max}(\sigma, 1) > \Omega_{\max}(\sigma, 2)$. Variation of Ω_{\max} with σ and m is similar to the JT disc.

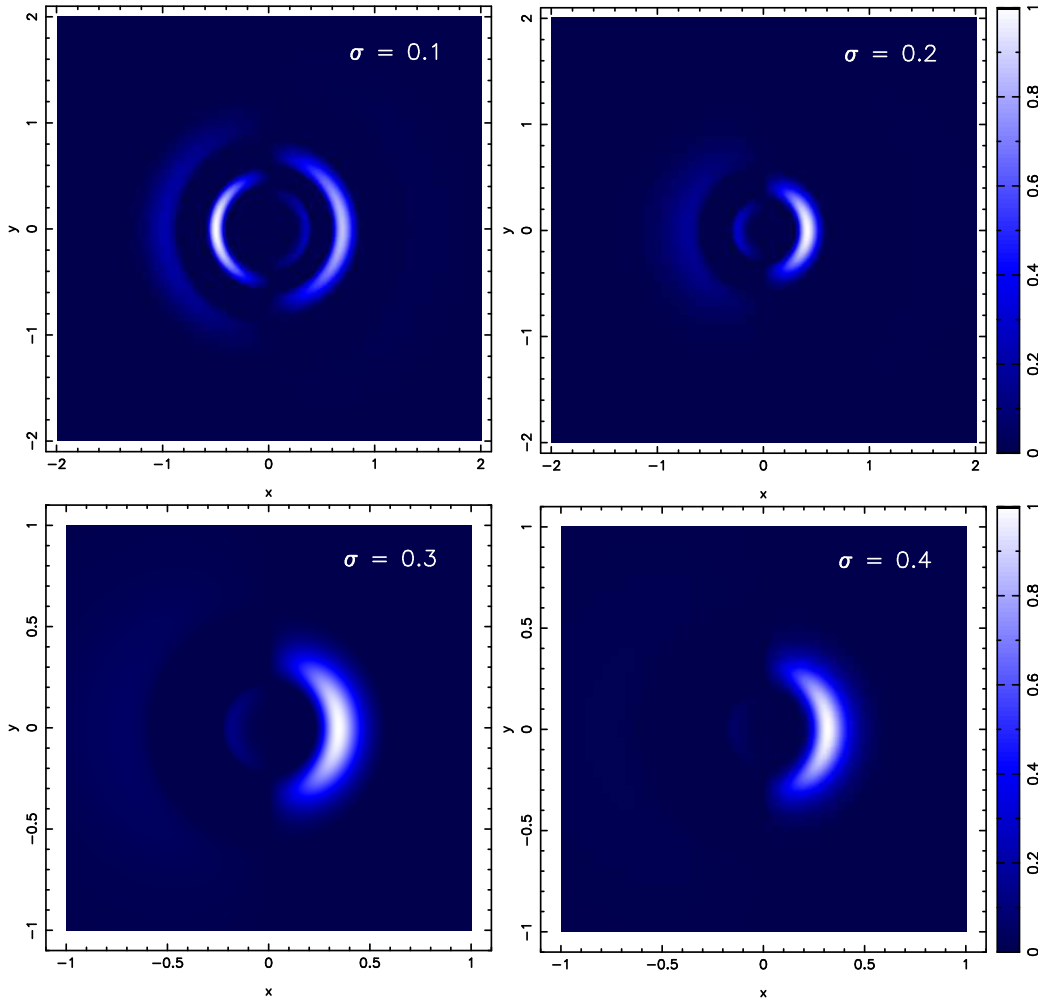


Figure 5. Patterns of oscillatory waves for JT annular disc. We have displayed the positive component of Real part of $\Sigma_1(R, \phi, t)$ at $t = 0$, for $m = 1$. Plots are for highest value of Ω_p for each value of σ and the panels are labelled for its respective σ values. The surface density is square normalized to unity in all panels and the color scheme for contours from 0 to 1 is plotted in a wedge on right side of the image.

We also solve the local WKB-dispersion relation (as given in the Appendix of Jalali & Tremaine (2012)) for the Kuzmin disc model. In Fig. 9 we compare the solution of local WKB dispersion relation and the eigenmodes calculated in this section for $\sigma = 0.1$. Top panel gives the integral equation solution and the lower panel gives eigenvalues obtained from local WKB dispersion relation. The eigenvalues differ from each other by about 20%, but qualitative trends are the same; for example, as we increase the value of m , the Ω_p value decreases, and Ω_p values increases with decreasing σ . Second one can be seen by comparing the plots for other σ values.

Figure 10, 11 and 12 are the plots of the perturbed surface density of the Kuzmin disc profile. In Fig. 10 we the plot $\Sigma_a(R)$ as a function R for $m = 1$. Plots are labelled for their σ and Ω_p values. $\Sigma_a(R)$ is normalized such that $\int dq \Sigma_a^2(R) = 1$. Figure 11 give images of

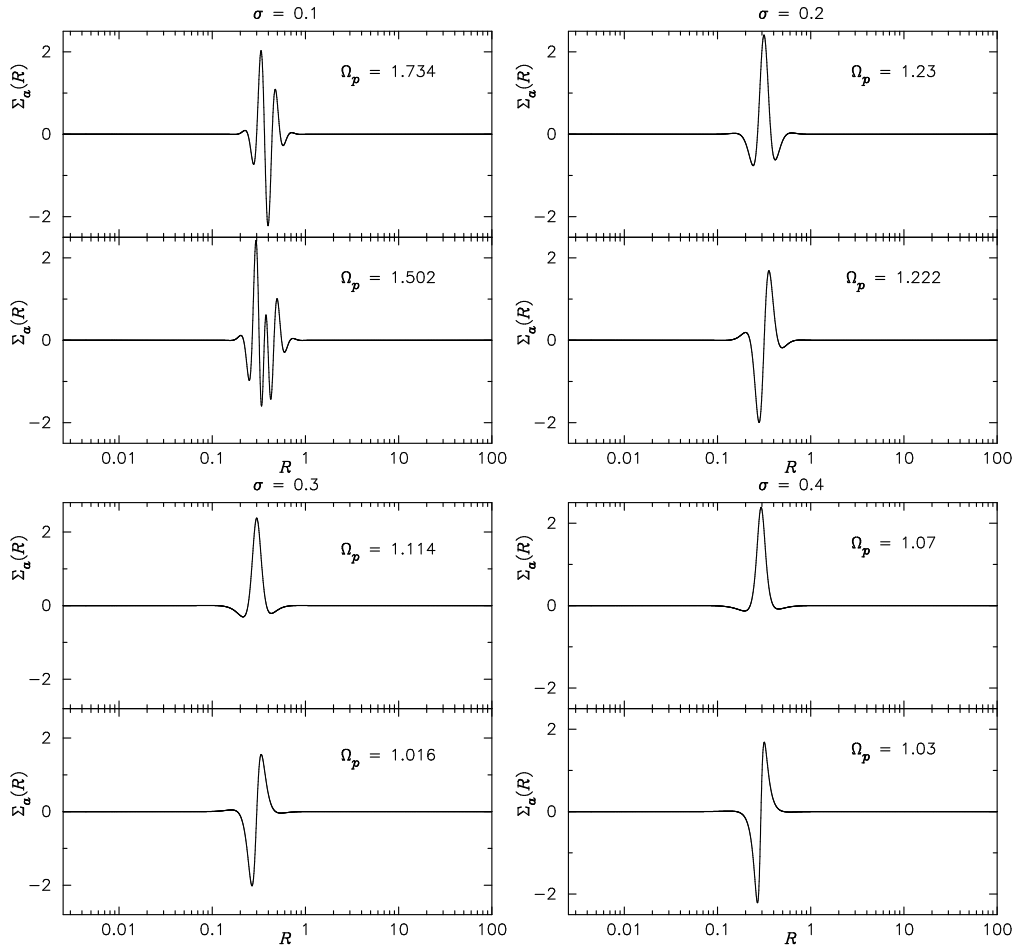


Figure 6. $\Sigma_a(R)$ vs R plot for $m = 2$ for two eigenmodes with least number of nodes, using Σ_d^{JT} as the unperturbed disc. Plots are labelled for their respective σ and Ω_p values.

density enhancement region, real part of $\Sigma_1(R, \phi, t)$, at $t = 0$ for the highest eigenvalue for each σ value used in Fig. 10. Color scheme and normalization used is same as that used in Fig. 5. Radial profile of square normalized wave functions $\Sigma_a(R)$ for $m = 2$ are given in Fig. 12. Apart from the exact forms of Σ_a for all cases, overall properties of the eigenfunctions are same as that we get using JT annular disc; (1) Number of nodes increase with decreasing Ω_p value, (2) wavefunctions are radially more compact for lower values of σ .

Next we compare the eigenvalues we get by solving the integral equation for the Kuzmin disc in this section with the solution of local WKB dispersion relation and the integral-equation solution for softened-gravity disc studied in Tremaine (2001). The model for velocity dispersion used in the present study directly corresponds to the one used by Tremaine (2001). In Table 1 we give the first five non-degenerate eigenvalues for all the three studies for $\sigma = 0.1$ and $m = 1$ (softening length $\beta = 0.1$ as used by Tremaine (2001)). First column is the local WKB-solution, second and third columns are for integral equation solution for

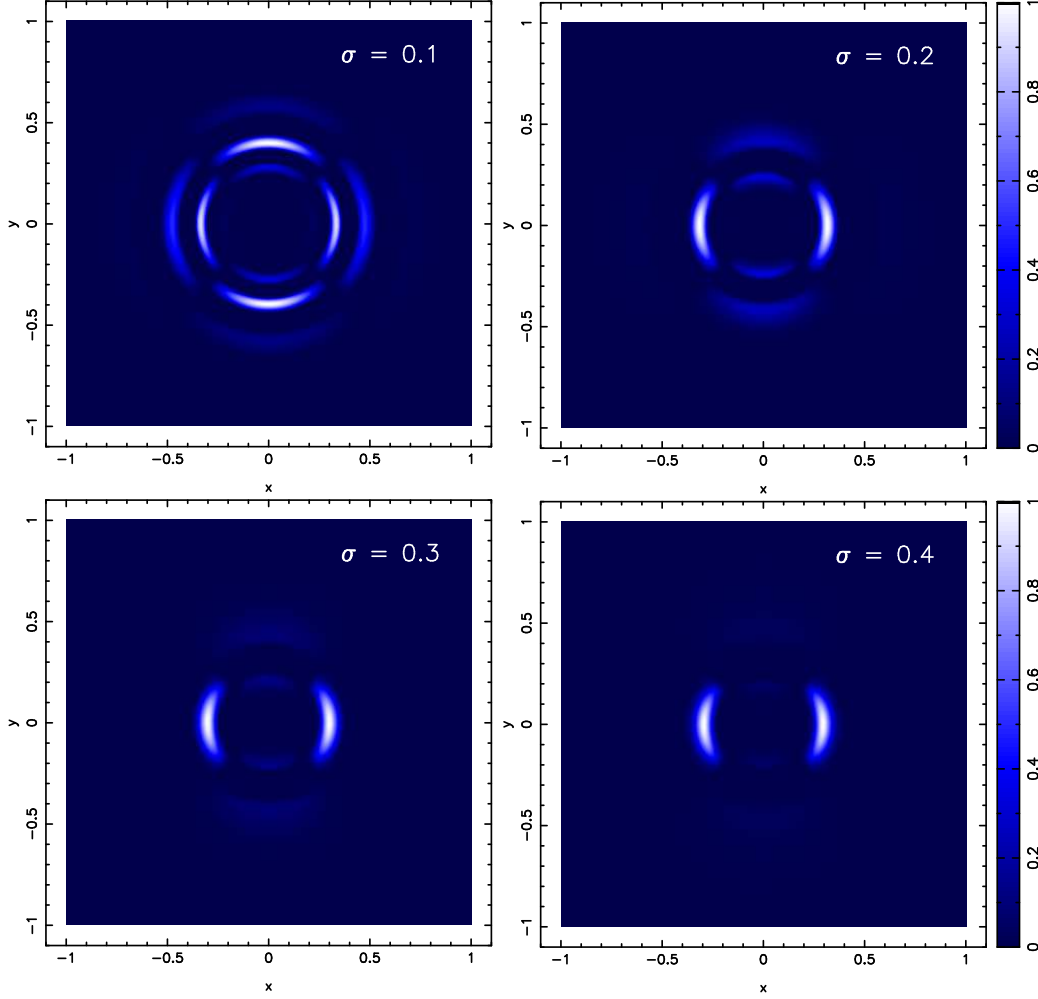


Figure 7. Image of positive component of Real part of $\Sigma_1(R, \phi, t)$ at $t = 0$ for the same set of parameters as in figure 6. Plots of the largest Ω_p for each σ value are displayed.

Solution for local WKB dispersion relation	Integral equation solution for softened gravity disc	Integral equation solution for collisionless disc
0.601	0.67	0.767
0.554	0.62	0.657
0.494	0.57	0.569
0.445	0.52	0.496
0.404	0.48	0.436

Table 1. Table of comparison between the solution of local WKB dispersion relation for Kuzmin disc, Integral equation solution for softened-gravity disc (Tremaine 2001) and Integral equation solution studied in the present chapter for Kuzmin disc. Values are for $\sigma = 0.1$.

softened-gravity disc and the collisionless discs, respectively. The eigenvalues match within $\sim 10\%$ and the match is within few percent for higher number of nodes, where the WKB approximation is expected to work better.

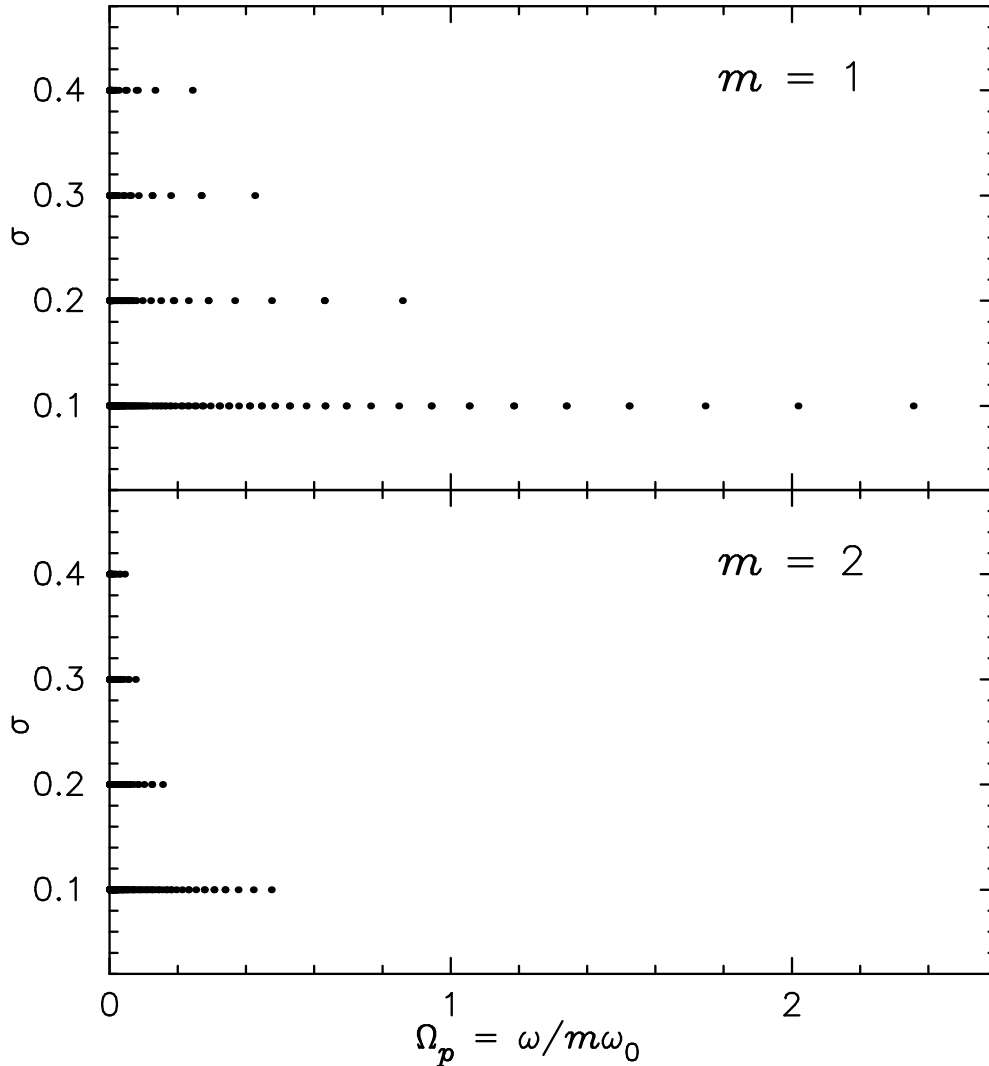


Figure 8. Plot of eigenvalues for Kuzmin disc profile. Horizontal axis is the pattern speed $\Omega_p = \omega/m\omega_0$, where ω_0 is the maximum of $|\dot{\varphi}|$ and the vertical axis is the σ value. Panels are labelled for their respective m values.

7 CONCLUSIONS

We have formulated linear perturbations in an axisymmetric collisionless stellar disc as an eigenvalue problem. By linearising the collisionless Boltzmann equation, we have derived an eigenvalue equation in the tight winding limit. We go a step further than the canonical WKB dispersion relation by treating the density-potential relation non-locally. This formalism allows us to determine both the eigenfrequencies as well as eigenfunctions for a stellar disc. We expect the accuracy of eigenvalues obtained through this formalism to be comparable to the WKB eigenvalues, which are fairly reasonable estimates of the eigenvalues as shown by Jalali & Tremaine (2012), but the advantages are: (1) We are able to obtain the eigenfunctions to a good accuracy, (2) and our formalism is considerably simpler than that of Jalali & Tremaine (2012).

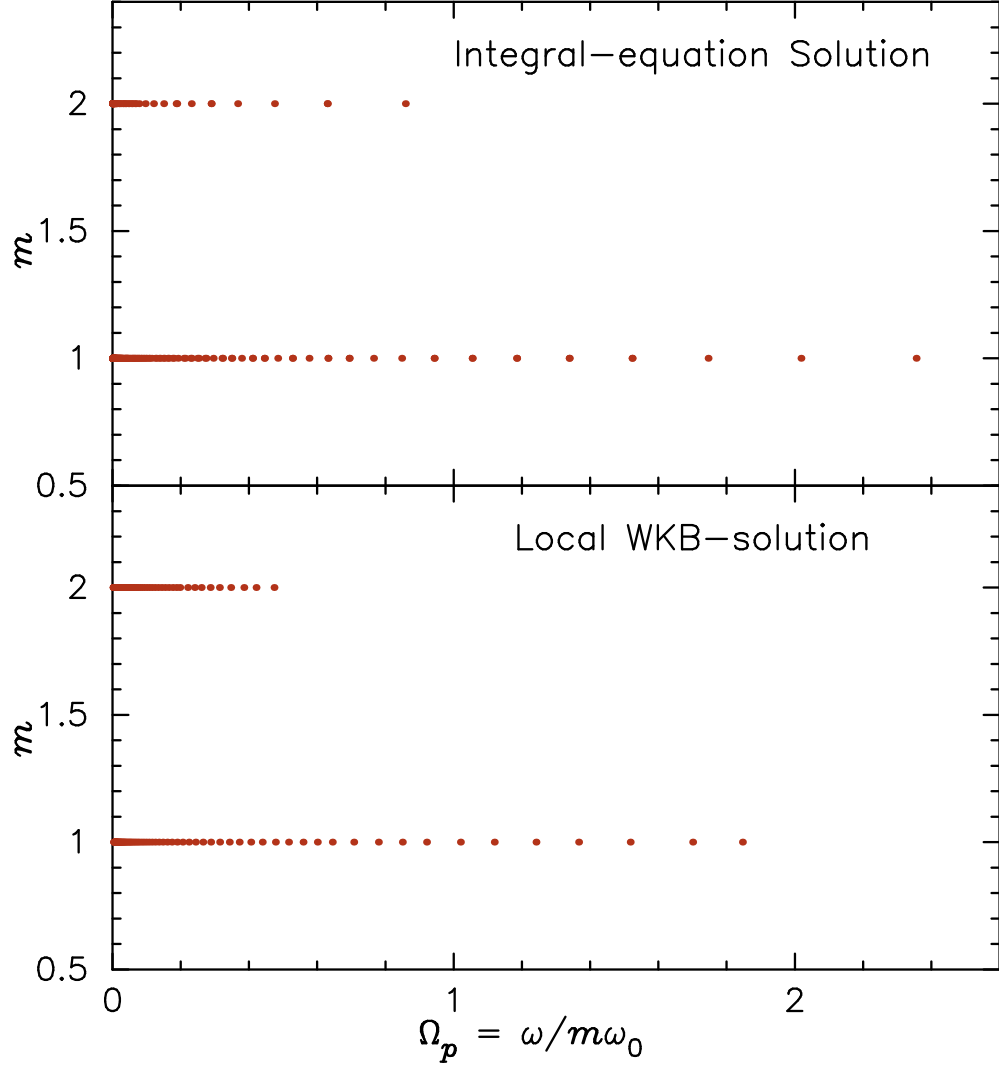


Figure 9. Comparison between the eigenvalues obtained by solving the local WKB dispersion relation and the eigenvalues calculated using the integral-equation for Kuzmin disc, with $\sigma = 0.1$. Horizontal and vertical axis are eigenvalue, Ω_p and m , respectively.

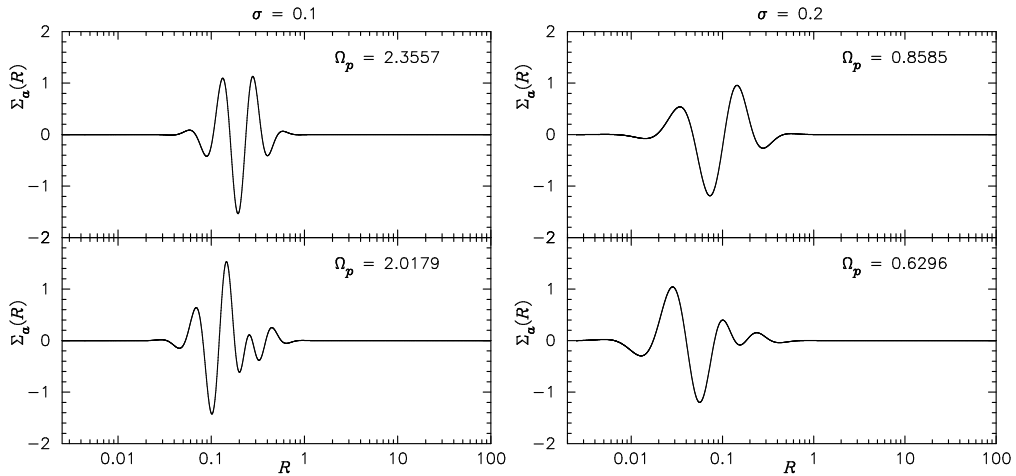


Figure 10. $\Sigma_a(R)$ vs R plot for $m = 1$, with Σ_d^{Kz} as the unperturbed density. Panels are labelled for their respective σ and Ω_p values. Normalization for $\Sigma_a(R)$ is same as used for JT annular disc.

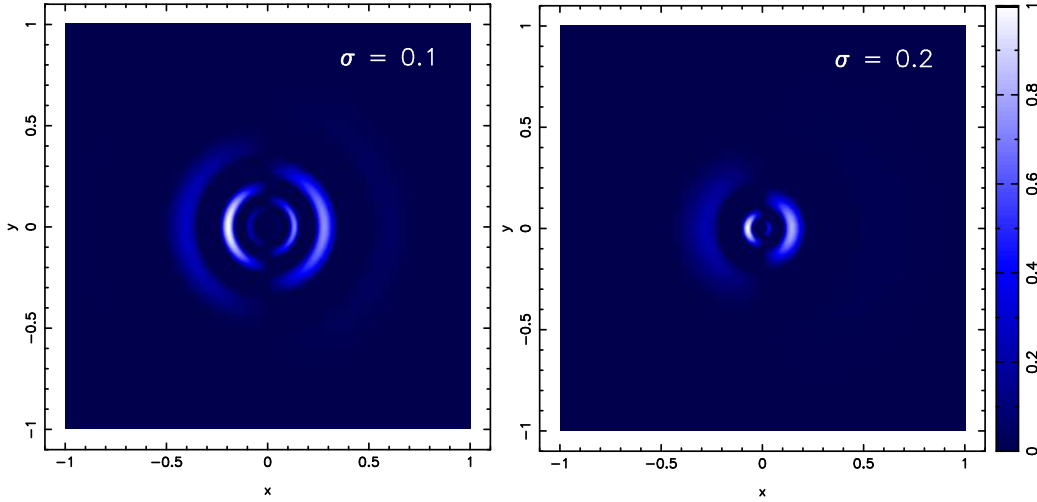


Figure 11. Image of positive part of the real component of $\Sigma_1(R, \phi, t)$ at $t = 0$, for highest eigenvalue for each σ value for the plots displayed in Fig. 10.

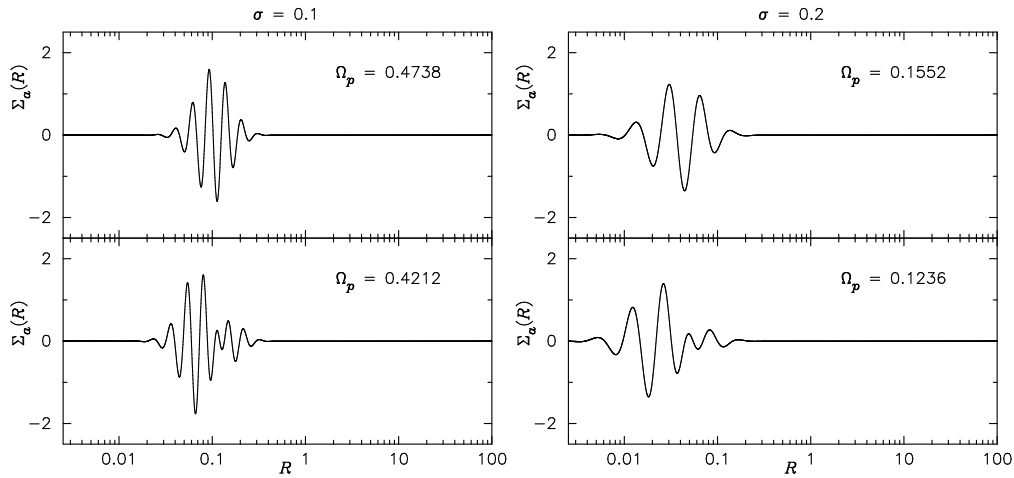


Figure 12. Square normalized eigenfunction $\Sigma_a(R)$ vs R plot for $m = 2$ for Kuzmin disc profile. Relevant labelling for σ and ω value is given in the plot.

Although our formulation is applicable to all stellar discs, for this work we have used it only to analyse the slow modes of a nearly Keplerian disc. We have calculated numerically the slow modes for two different unperturbed surface density profiles, namely: (1) JT annular disc, (2) and the Kuzmin disc. Radial profile of velocity dispersion was assumed to be $\sigma_R(R) = \sigma R \kappa(R)$, where $\sigma < 1$ is a constant. This is a reasonable model for velocity dispersion (Jalali & Tremaine 2012). Our conclusions for the slow modes of these two discs are:

- Since the kernel of the slow mode integral-eigenvalue problem is symmetric, therefore all the eigenvalues are real. Moreover all the non-singular eigenvalues are prograde, $\Omega_p > 0$.

- The important trends seen by varying σ are: (a) Largest eigenfrequency is a decreasing function of σ , (b) and the number of non-singular eigenvalues increases as σ decreases.
- $\Omega_{\max}(\sigma, m)$ value decreases as we go from $m = 1$ to 2. In addition, for a given Ω_p value, number of nodes for $m = 1$ are larger than that for $m = 2$. In other words eigenfunctions are more radially compact for $m = 1$.
- The general behaviour of the eigenfunctions is that: (1) The wavelength of oscillations decreases with decreasing pattern speed, (2) the number of nodes increase with decreasing Ω_p values, (3) and wavefunctions are radially more compact for lower values of σ .
- Largely the behaviour of the eigenfrequencies and the eigenfunctions is similar for the two unperturbed surface density chosen, but there are quantitative differences, such as the values of pattern speeds. In the case of Kuzmin disc all $\Omega_p > 0$ are found to be non-singular, although there is a continuum of eigenvalues close to $\Omega_p = 0$; whereas in the case of JT annular discs the eigenvalues with $\Omega_p \leq 1$ are all singular modes.

These conclusions are consistent with the earlier works of Tremaine (2001); Gulati et al. (2012); Jalali & Tremaine (2012). Since the slow modes are stable, the excitation mechanism for such modes is important; for example, a close encounter with a passing, massive object can act as an external perturbation that can excite these modes. Jalali & Tremaine (2012) have considered such a phenomenon in detail and conclude that external perturbation is an excellent mechanism to excite the slow modes.

Slow modes exists with arbitrary azimuthal wavenumber m but the modes with lower m values are large scale and hence are most prominent in the observations. Also lower m modes are easy to excite, for example by an external perturber (Jalali & Tremaine 2012). As noted by Jalali & Tremaine (2012), galactic discs surrounding a supermassive BH and debris disc around stars are similar in the sense that dynamics of both the discs are influenced by the central object (star/supermassive BH) and the self-gravity of the disc. Hence the analysis presented in this paper is also applicable to debris disc. Jalali & Tremaine (2012) proposed that most of the non-axisymmetric features in the debris disc may be due to slow modes. There are other hypothesis like a presence of massive planet in debris discs, which can also cause these asymmetries in the discs. These can be distinguished from slow modes if the structures are observed for long enough time or with higher resolutions. Features due to slow modes will rotate much slower as compared to the angular speed of the disc whereas structures due to planets in the discs will rotate at a speed comparable to the angular speed.

Double peak stellar distribution is observed in two galaxies: M31 and NGC4486B. Distribution in both these galaxies differ from each other, for instance, both the peaks in NGC4486B are symmetric w.r.t. the photocenter in contrast to the peaks in M31. Double peak stellar distribution in NGC4486B is more likely to be due to $m = 2$ modes rather than $m = 1$ eccentric modes for M31. Both these galaxies being different morphologically can excite different m -modes predominantly. These eccentric modes may also play an important role in feeding the central BH in galaxies.

APPENDIX A: THE LOCAL LIMIT

Here we verify that a local approximation—valid when $|\alpha|$ is not just much larger than m , but is truly large—to the integral problem reduces it to the well-known WKB dispersion relation of Toomre (1964).

We first solve the integrals over ‘ q' ’ (in particular solve the q' integral in A_m , equation (20)) and ‘ α ’ in Σ_a (equation (40)) using the *stationary phase* approximation (Lighthill 2001). For an oscillatory integral with rapidly changing phase, most of the contribution to the integral cancels due to destructive superposition of oscillatory functions. Therefore, the phase can be approximated by its Taylor expansion around the stationary phase point, that is the point at which phase change is zero. In addition, the non-oscillatory part of the integrand is simply replaced by its value at the stationary point.

We begin by writing $\Sigma_a(R)$ as

$$\Sigma_a(R) = h(R) \exp \left[i \int^R k(R'') dR'' \right]. \quad (\text{A1})$$

This essentially divides $\Sigma_a(R)$ into a slowly varying function $h(R)$ of R and a fast varying oscillatory function of R . Substituting this in equation (20) we get,

$$A_m(\alpha) = \int_{-\infty}^{\infty} dq' R'^{3/2} h(R') \exp(i\psi), \quad (\text{A2})$$

where $\psi = \int^R k(R'') dR'' - \alpha q'$, is the phase of the oscillatory part of the integral over q' . Any point $R = R_*$ (or equivalently $q = q_*$) is called a stationary point if at $q = q_*$, $d\psi/dq = 0$, which when substituted for ψ gives the condition, $R_* k(R_*) = \alpha$. Since the phase is nearly constant at the stationary point (which in turn gives the leading contribution to the integral), we shall replace $\psi(R)$ with its Taylor expansion around R_* ,

$$\psi(R) = \psi(R_*) + (q - q_*)^2 \varrho,$$

where, $\varrho = R_*^2 (dk/dR|_{R_*} + \alpha/R_*^2)/2$. We retain terms up to second order in the Taylor

expansion. Other parts of the integrand are replaced by their value at R_* and can be taken out of the integral. All this put together in the expression of A_m given in Eq. (A2) gives,

$$\begin{aligned} A_m(\alpha) &= R_*^{3/2} \Sigma_a(R_*) \exp[-i\alpha q_*] \int_{-\infty}^{\infty} dq' \exp[i(q' - q_*)^2 \varrho] , \\ &= R_*^{3/2} \Sigma_a(R_*) \exp[-i\alpha q_*] \left[\sqrt{\frac{\pi}{|\varrho|}} \exp\left[i \operatorname{sgn}(\varrho) \frac{\pi}{4}\right] \right] . \end{aligned} \quad (\text{A3})$$

For the second equality above we have used the Gaussian integral,

$$\int_{-\infty}^{\infty} dx \exp[\pm i\lambda x^2] = \sqrt{\frac{\pi}{|\lambda|}} \exp\left[\pm i \operatorname{sgn}(\lambda) \frac{\pi}{4}\right] , \quad (\text{A4})$$

and $\operatorname{sgn}(\lambda)$ is the sign of λ . We next use this value of $A_m(\alpha)$ in the expression of Σ_a^{dt} given in equation (31) and the fact that $\Sigma_a = \Sigma_a^{\text{dt}}$ (because the indirect term equals zero for the present formulation), to get

$$\begin{aligned} \Sigma_a(R) &= \frac{2G\Sigma_d}{R^{5/2}\kappa^2} \sum_{n=1}^{\infty} \left(\frac{n^2}{n^2 - s^2} \right) \int_{-\infty}^{\infty} \frac{d\alpha}{2\pi} N(\alpha, m) R_*^{3/2} h(R_*) e^{-\chi} \times \\ &\times \left[B_n \sqrt{\frac{\pi}{|\varrho|}} \exp\left(i \operatorname{sgn}(\varrho) \frac{\pi}{4}\right) \right] \exp[i\varphi] , \end{aligned} \quad (\text{A5})$$

where the phase $\varphi = \int^{R_*} k(R'') dR'' - \alpha(q_* - q)$. At the stationary phase point $d\varphi/d\alpha = 0$, which on substitution of φ , gives the stationary phase point as $q = q_*$ or $R = R_*$. Hence integral over α in above equation, on applying the stationary phase approximation, simplifies to

$$\begin{aligned} \Sigma_a(R) &= \frac{G\Sigma_d}{\pi R^{5/2}\kappa^2} \sum_{n=1}^{\infty} \left(\frac{n^2}{n^2 - s^2} \right) N(kR, m) R_*^{3/2} \Sigma_a(R) B_n(\alpha, \chi) \times \\ &\times \sqrt{\frac{\pi}{|\varrho|}} \exp\left(i \operatorname{sgn}(\varrho) \frac{\pi}{4}\right) \int_{-\infty}^{\infty} d\alpha e^{-i\alpha^2 \varsigma} , \\ &= \frac{2G\Sigma_d}{2R\kappa^2} \sum_{n=1}^{\infty} \left(\frac{n^2}{n^2 - s^2} \right) N(kR, m) \Sigma_a(R) B_n(\alpha, \chi) \times \\ &\times \sqrt{\frac{1}{|\varrho\varsigma|}} \exp\left[i \left(\operatorname{sgn}(\varrho) \frac{\pi}{4} - \operatorname{sgn}(\varsigma) \frac{\pi}{4} \right)\right] . \end{aligned} \quad (\text{A6})$$

Here ς is defined as $(1/2R_*)(dR_*/d\alpha)$ and equation (A4) is used to write the second equality. It can be noted from the definitions of ϱ and ς that:

- (i) $\varrho\varsigma = \frac{1}{4}$, and
- (ii) $\operatorname{sgn}(\varrho) = \operatorname{sgn}(\varsigma)$.

Both these relation are obtained using $\alpha = R_*k(R_*)$, which was derived earlier. The standard WKB approximation is $|kR| \gg m$. Also $kR = \alpha$ at the stationary phase point. This gives an equivalent condition for WKB as $|\alpha| \gg m$. The asymptotic form of $N(\alpha, m)$ for $\alpha \gg m$

is

$$N(\alpha, m) \sim \frac{2\pi}{(\alpha^2 + m^2)^{1/2}} \sim \frac{2\pi}{|\alpha|}. \quad (\text{A7})$$

All these put together reduce equation (A6) to

$$\Sigma_a(R) = \frac{2\pi G \Sigma_d |k|}{\kappa^2} \sum_{n=1}^{\infty} \left(\frac{n^2}{n^2 - s^2} \right) \frac{2}{\chi} e^{-\chi} I_n(\chi) \Sigma_a(R), \quad (\text{A8})$$

which implies

$$\kappa^2 - (\omega - m\Omega)^2 = 2\pi G \Sigma_d |k| \mathcal{F}(s, \chi), \quad (\text{A9})$$

where

$$\mathcal{F}(s, \chi) = \frac{2}{\chi} (1 - s^2) e^{-\chi} \sum_{n=1}^{\infty} \frac{I_n(\chi)}{1 - s^2/n^2}. \quad (\text{A10})$$

Thus we find that in the local approximation our equation reduces to the standard WKB dispersion relation (Toomre 1964; Binney & Tremaine 2008).

ACKNOWLEDGEMENTS

We would like to thank S. Sridhar for many useful discussions during the course of this work.

REFERENCES

- Anderson et. al. 1999, LAPACK Users' Guide (3rd ed., Society for Industrial and Applied Mathematics)
- Binney, J., & Tremaine, S. 2008, Galactic Dynamics (2ed., Princeton: Princeton University Press)
- Clampin, M., Krist, J. E., Ardila, D. R., et al. 2003, *Astron. J.*, 126, 385
- Goldreich, P., & Tremaine, S. 1979, *Astroph. J.*, 233, 857
- Gulati, M., Saini, T. D., & Sridhar, S. 2012, *Mon. Not. Roy. Ast. Soc.*, 424, 348
- Heap, S. R., Lindler, D. J., Lanz, T. M., et al. 2000, *Astroph. J.*, 539, 435
- Jalali, M. A., & Tremaine, S. 2012, *Mon. Not. Roy. Ast. Soc.*, 421, 2368
- Kalnajs, A. J. 1971, *Astroph. J.*, 166, 275
- Lauer, T. R., Faber, S. M., Groth, E. J., et al. 1993, *Astron. J.*, 106, 1436
- Lauer, T. R., Tremaine, S., Ajhar, E. A., et al. 1996, *Astrophysical. J. Letters*, 471, L79
- Lighthill, J. 2001, *Waves in Fluids*, by James Lighthill, pp. 520. ISBN 0521010454. Cambridge, UK: Cambridge University Press, December 2001.,

- Marsh, K. A., Dowell, C. D., Velusamy, T., Grogan, K., & Beichman, C. A. 2006, *Astrophysical J. Letters*, 646, L77
- Press, W. H., Teukolsky, S. A., Vetterling, W. T., & Flannery, B. P. 1992, *Numerical Recipes* (2nd ed., Cambridge: University Press)
- Reichard, T. A., Heckman, T. M., Rudnick, G., et al. 2009, *Astroph. J.* , 691, 1005
- Sridhar, S., & Saini, T.D. 2010, *Mon. Not. Roy. Ast. Soc.*, 404, 527
- Telesco, C. M., Fisher, R. S., Piña, R. K., et al. 2000, *Astroph. J.* , 530, 329
- Toomre, A. 1963, *Astroph. J.* , 138, 385
- Toomre, A. 1964, *Astroph. J.* , 139, 1217
- Tremaine, S. 2001, *Astron. J.*, 121, 1776